3D Motion Analysis of Keratin Filaments in Living Cells

Article *in* Proceedings of SPIE - The International Society for Optical Engineering · March 2010

DOI: 10.1117/12.844148

Lehrstuhl für Bildverarbeitung
Institute of Imaging & Computer Vision

3D Motion Analysis of Keratin Filaments in Living Cells

Gerlind Herberich and Reinhard Windoffer and Rudolf Leube and Til Aach

Institute of Imaging and Computer Vision
RWTH Aachen University, 52056 Aachen, Germany
tel: +49 241 80 27860, fax: +49 241 80 22200
web: www.lfb.rwth-aachen.de

Institute of Molecular and Cellular Anatomy
RWTH Aachen University, 52056 Aachen, Germany
tel: +49 241 80 89107, fax: +49 241 80 82 508
web: www.moca.rwth-aachen.de

in: Medical Imaging 2010: Image Processing. See also BibTeX entry below.

BibTeX:

```
@inproceedings{HER10a,
  author = {Gerlind Herberich and Reinhard Windoffer and Rudolf Leube and Til Aach},
  title = {{3D} Motion Analysis of Keratin Filaments in Living Cells},
  booktitle = {Medical Imaging 2010: Image Processing},
  editor = {},
  publisher = {SPIE Vol.\ 7623},
  address = {San Diego, USA},
  month = {February 13--18},
  year = {2010},
  pages = {accepted}}
```


document created on: March 3, 2010
created from file: HER10a.tex
cover page automatically created with CoverPage.sty
(available at your favourite CTAN mirror)

RWTH AACHEN
RHEINISCH-WESTFÄLISCHE TECHNISCHE HOCHSCHULE AACHEN

3D Motion Analysis of Keratin Filaments in Living Cells

Gerlind Herberich[a], Reinhard Windoffer[b], Rudolf Leube[b] and Til Aach[a]

[a]Institute of Imaging & Computer Vision, RWTH Aachen University,
D-52056 Aachen, Germany

[b]Institute of Molecular & Cellular Anatomy, University Hospital Aachen,
D-52074 Aachen, Germany

ABSTRACT

We present a novel and efficient approach for 3D motion estimation of keratin intermediate filaments in vitro. Keratin filaments are elastic cables forming a complex scaffolding within epithelial cells. To understand the mechanisms of filament formation and network organisation under physiological and pathological conditions, quantitative measurements of dynamic network alterations are essential. Therefore we acquired time-lapse series of 3D images using a confocal laser scanning microscope. Based on these image series, we show that a dense vector field can be computed such that the displacements from one frame to the next can be determined. Our method is based on a two-step registration process: First, a rigid pre-registration is applied in order to compensate for possible global cell movement. This step enables the subsequent nonrigid registration to capture only the sought local deformations of the filaments. As the transformation model of the deformable registration algorithm is based on Free Form Deformations, it is well suited for modeling filament network dynamics. The optimization is performed using efficient linear programming techniques such that the huge amount of image data of a time series can be efficiently processed. The evaluation of our results illustrates the potential of our approach.

Keywords: Motion analysis, registration, cytoskeleton, confocal laser scanning microscopy, fluorescence microscopy.

1. INTRODUCTION

4D (3D+time) live cell fluorescence imaging by means of confocal laser scanning microscopy has become a widely used tool in cell biology for the analysis of the dynamics of subcellular structures. In the work presented here, we investigate the dynamic processes that keratin intermediate filaments (KFs) exhibit. KFs as part of the cytoskeleton are responsible for the mechanical stability of epithelial cells and tissues and are also involved in the regulation of many basic cell functions.[1] They are flexible, filamentous structures of about 10nm diameter. Built from proteins that polymerize primarily at the cell periphery, they first elongate, integrate into the peripheral network and move toward the nucleus where they may disassemble for reutilization in another assembly-disassembly cycle.[2–4]

Under pathological conditions this cycle of filament and network formation may be disturbed. Mutations in keratin genes lead to diverse diseases such as Epidermolysis bullosa simplex. In order to gain new insights into the underlying mechanisms, a better understanding of the keratin network organisation under physiological and pathological conditions is needed.

For this purpose a precise quantitative motion analysis in 3-dimensional space is indispensable. Related work includes Quantitative Fluorescent Speckle Microscopy by Danuser et al.[5] where speckles instead of filaments were analyzed. In [6] the dynamics of vimentin intermediate filaments were analyzed by dividing the image into blocks and computing a correlation coefficient-based displacement index for each block. Furthermore, there has

Further author information: (Send correspondence to Gerlind Herberich)
Gerlind Herberich: E-mail: gerlind.herberich@lfb.rwth-aachen.de, Telephone: +49 241 80-27974
Reinhard Windoffer: Email: rwindoffer@ukaachen.de, Telephone: +49 241 80-89998
Rudolf Leube: Email: rleube@ukaachen.de, Telephone: +49 241 80-89108
Til Aach: E-mail: til.aach@lfb.rwth-aachen.de, Telephone: +49 241 80-27860

been work on measuring the velocity of *single* actin filaments utilizing - after denoising - an active contour-based segmentation followed by a tracking algorithm.[7] None of these studies attempted the computation of a dense 3-dimensional displacement vector field for each object point to characterize the motion of both single filaments and filaments integrated into a network.

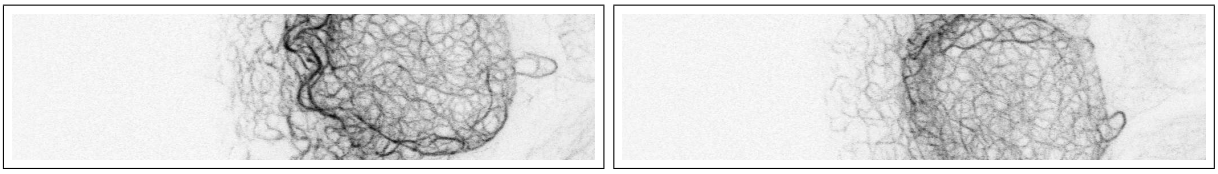

Figure 1. Projection of the 3D keratin filament network fluorescence detected within a cell segment at the beginning (left) and at the end (right) of a time series illustrating global cell movement superimposed to local filament motion.

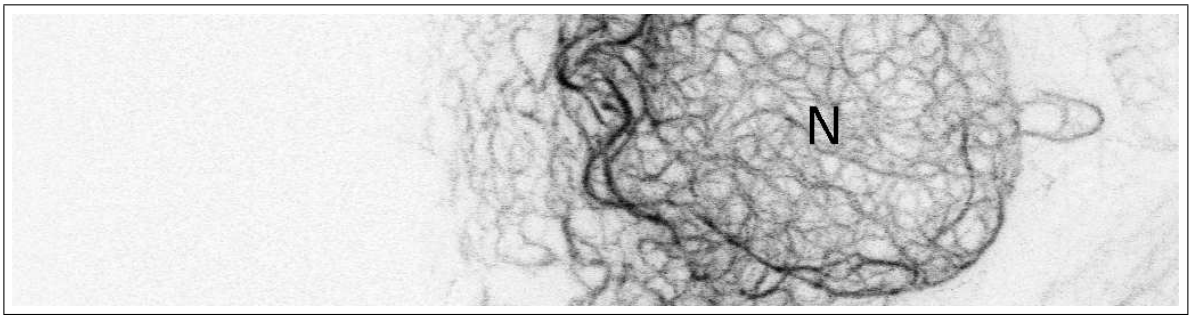

Figure 2. Screenshot of video: Projection of the 3D keratin filament network fluorescence detected within a cell (N: nucleus). On the left hand side, the motion of the filaments from cell periphery towards cell interior can be observed. http://dx.doi.org/doi.number.goes.here

To this end, we propose a two-step registration procedure. This is based on the observation that the sought motion of the filaments may be superimposed by a global movement of the cell as a whole (see figure 1 for illustration). The video in figure 2 illustrates the movements typically contained in the image data. Our goal is to compensate for such global cell movement in a first step, such that the local movements of the filaments can be quantified in a second step. This compensation is realized by an intensity-based rigid pre-registration consisting of a translational and a rotational part. Based on these pre-registered images, the local motion of the filaments is then estimated. Given the shape-changing nature of the KFs, it is obvious that only a nonrigid registration method can precisely capture the sought motion. A nonrigid registration algorithm[8,9] based on cubic B-spline Free Form Deformations (FFD)[10] accounts for the flexibility of the filaments while providing a computationally efficient estimation. This is crucial in view of the vast amount of image data to be analyzed. A further step towards a computationally efficient algorithm consists of a graph-cuts-based optimization that relies on linear programming techniques.[11,12]

The remainder of our paper is organized as follows. The image acquisition process and the data characteristics are described in section 2. Section 3 introduces the nonrigid registration algorithm applied. An evaluation of the results is given in section 4. Section 5 provides closing remarks and presents prospects for the future.

2. IMAGE ACQUISITION

The starting point of our spatiotemporal analysis consists of monitoring living cultured cells with fluorescently labeled keratins over time by means of confocal laser scanning microscopy.[13,14] We acquired time series of 3D images or rather, image stacks, one such stack being composed of 2D slices each at a different focal plane or depth of the specimen (see figure 3). The ideal fluorescence microscopy time series requires high spatio-temporal sampling, high signal-to-noise ratio (SNR) and long observation time.[15] However, increasing the sampling rate or signal intensity increases photodamage[13] of the fluorophores which may finally lead to cell death. Thus,

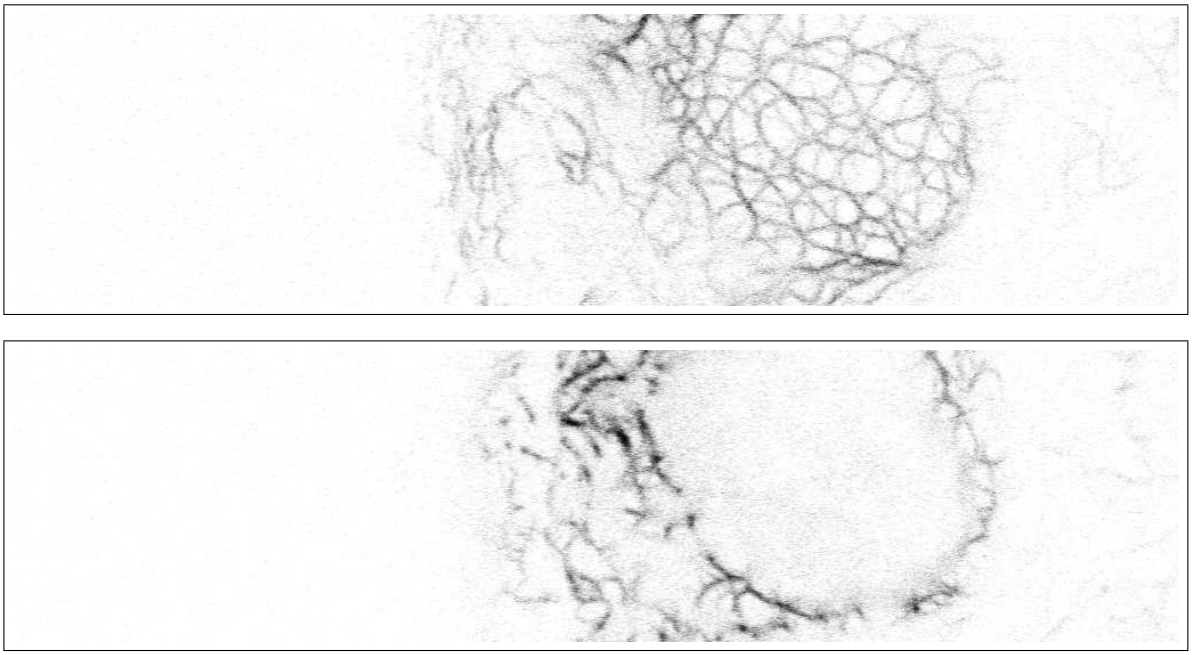

Figure 3. Keratin filament network of one cell - 2D slices at different depths of the specimen. Top: bottom of the cell with the network formed by the keratin filaments. Bottom: middle region of the cell showing the filament network around the cell nucleus which appears in the image as structureless ellipsoidal area.

these competing requirements cannot be met simultaneously and a suitable trade-off has to be found. Towards an optimal trade-off, the temporal resolution was empirically determined to be 60 seconds between consecutive frames and the spatial resolution to be 60 nm per voxel in the image plane and 500 nm per voxel along the optical axis. This leads to a comparatively poor resolution in the third dimension. A further aggravating factor for the automated image analysis is the corruption of the image data by photon counting noise due to the very low fluorescence signal.

3. REGISTRATION ALGORITHM

The basic idea behind motion estimation by image registration is that image points x are translated from one frame to the next while their brightness I follows a certain relationship, linear or nonlinear. In our application we assumed brightness constancy. The process of motion estimation then consists of finding for each image point x a motion vector $\tau(x)$ such that

$$I_t(x) = I_{t+1}(x + \tau(x)). \tag{1}$$

If the displacement τ corresponds to the true displacement for all image points, and in the ideal case of noise free data, the difference between the two frames will be zero. Thus, the optimal transformation $\hat{\tau}$ is the transformation that minimizes a suitable difference measure f for all image points:

$$\hat{\tau} = \arg\min(\sum_x f(I_t(x), I_{t+1}(x + \tau(x)))). \tag{2}$$

An appropriate difference measure under the assumption of brightness constancy is the Sum of Absolute Differences (SAD) or the Sum of Squared Differences (SSD).

To simplify the algorithm, we use here an approach to deformable registration[8,9] that relies on a discrete deformation grid. Then only the displacements $\tau(p)$ for a discrete set of grid points $p \in \mathcal{G}$ are optimized. Afterwards, an interpolation strategy is used to determine the displacements for the image points lying between the grid points:

$$\tau(x) = \sum_p \eta(|x - p|)\tau(p) \tag{3}$$

where η is a weighting function controlling the influence of the displacement $\tau(p)$ of grid point p on the displacement assigned to image point x depending on the distance of x from p.

To find the optimal displacement for all grid points, we thus have to minimize

$$C_{data}(\tau) = \sum_p \sum_x \eta(|x-p|) f(I_t(x), I_{t+1}(x+\tau(x))), \tag{4}$$

such that for each grid point the difference measure f is evaluated for all image points lying within the support of η.

In order to best capture the deformations of the filaments, we choose cubic B-splines as interpolator. Cubic B-splines-based FFDs[10] have succesfully been applied in a variety of nonrigid registration methods.[16] The idea behind FFDs is to deform an object by manipulating an underlying grid of control points. Due to the local support of the basis functions of B-splines, the transformation model is then locally controlled. In other words, changing the displacement of a point only affects the transformation in the neighborhood of that point. Equation (4) shows that this formulation of the registration problem leads to a local optimization of the difference measure for each grid point such that small local deformations can well be captured.

However, simply minimizing the above criterion will not lead to an appropriate estimate of the sought motion as the number of variables is larger than the number of constraints: For each image point a three-dimensional vector is sought while only one constraint - namely the gray value difference - is available. This makes dense deformable image registration an ill-posed problem[17] per se.

To cope with the ill-posedness of the problem, we augment our minimization criterion with a regularization term.[18] While the minimization of equation (4) can be considered as the driving force of the registration, the regularizer controls the transformation[19] and thus confines the solution space. In our case, regularization consists of the introduction of smoothness constraints on the deformation field as KFs behave like elastic cables. In mathematical terms, smoothness can be enforced by penalizing high derivatives of grid deformation. Here, only the first derivative is accounted for such that small deformations are favored over large deformations while curvature is not taken into account. As only displacements at grid points are considered during optimization, the first derivative is approximated by a finite difference on the discrete grid:

$$C_{smooth}(\tau) = \sum_p \sum_{q \in \mathcal{N}(p)} |\tau(p) - \tau(q)|, \tag{5}$$

with $q \in \mathcal{N}(p)$ being all grid points in the neighborhood of grid point p. The complete formulation of the registration problem then becomes

$$\hat{\tau} = \arg\min(C_{data}(\tau) + \mu C_{smooth}(\tau)), \tag{6}$$

where μ is a weighting factor determining the trade-off between data term and the imposed smoothness of the tranformation.

From a Bayesian point of view, this estimate can be interpreted as the maximum-a-posteriori estimate of τ. According to Bayes' rule

$$p(\tau|I_t, I_{t+1}) \propto p(I_t, I_{t+1}|\tau)p(\tau) \tag{7}$$

with $p(I_t, I_{t+1}|\tau)$ being the likelihood function of τ and $p(\tau)$ its prior. Maximizing the posterior can be achieved by maximizing the $log(p(\tau|I_t, I_{t+1}))$ as the logarithm is a continuously increasing function. Thus, the maximum-a-posteriori estimate is given by

$$\hat{\tau} = \arg\min(-\log(p(I_t, I_{t+1}|\tau)) - \log(p(\tau))) \tag{8}$$

where the first term plays the same role as the data term in equation (6) and the second term the role of the smoothness term needed to favor expected transformations respectively.

In the following, we will state how to efficiently minimize the criterion in equation (8) without computation of its derivative. To this end, the search space is quantized into a discrete set of displacements, each assigned

with a unique label. The task then becomes to assign a label $l \in \mathcal{L}$ to each grid point, $\mathbf{l} : \mathcal{G} \rightarrow \mathcal{L}$, such that criterion 8 is minimized. In other words, the optimal transformation is then given by the optimal labeling $\hat{\mathbf{l}}$ - the problem becomes a labeling problem:

$$\hat{\mathbf{l}} = \arg\min(-\log(p(I_t, I_{t+1}|\mathbf{l})) - \log(p(\mathbf{l}))). \tag{9}$$

To further specify this probabilistic version of the minimization criterion, we need to relate likelihood and prior to the previously defined cost measures of data and smoothness term. $C_{data}(\tau)$ and $C_{smooth}(\tau)$ represent the costs associated with transformation τ. The higher this cost, the less likely the transformation. We can encode this by rewriting likelihood and prior in terms of a Gibbs distribution[20]

$$p(\mathbf{l}) = \frac{1}{Z} e^{-\frac{1}{T}U(\mathbf{l})} \tag{10}$$

where Z is a normalizing constant (called the partition function), T the so-called temperature which will be set to 1 here and $U(\mathbf{l})$ the energy function. Thus, the smaller the energy or cost respectively associated with labeling $\mathbf{l}$, the more likely the labeling is. The likelihood then becomes

$$p(I_t, I_{t+1}|\mathbf{l}) \propto e^{-U(I_t, I_{t+1}|\mathbf{l})} \tag{11}$$

and the prior

$$p(\mathbf{l}) \propto e^{-U(\mathbf{l})} \tag{12}$$

such that equation (9) becomes

$$\hat{\mathbf{l}} = \arg\min(U(I_t, I_{t+1}|\mathbf{l}) + U(\mathbf{l})). \tag{13}$$

The energy function is defined as sum of clique potentials V_c over all possible cliques C

$$U(\mathbf{l}) = \sum_{c \in C} V_c(\mathbf{l}) \tag{14}$$

such that we can specify likelihood and prior energy in the deformation grid domain as follows: Concerning the likelihood energy or the data cost respectively, recall that according to equation (4) it can be determined by considering for each grid point the image points in its neighborhood without accounting for neighboring grid points. Regarding the deformation grid, this can naturally be expressed as a clique of size one which encodes the idea that within our locally controlled transformation model the data cost associated with displacing one grid point is statistically independent from the data cost associated with the displacements of neighboring grid points. For the specification of the prior energy, we need to consider neighboring grid points. Therefore we use a clique of size two. Equation (13) can then be reformulated as follows

$$\begin{aligned} \hat{\mathbf{l}} &= \arg\min(\sum_{p \in \mathcal{G}} V_p(l_p) + \sum_{(p,q) \in \mathcal{E}} w_{pq} V_{pq}(l_p, l_q)) \\ &= \arg\min(\sum_{p \in \mathcal{G}} V_p(l_p) + \sum_{p \in \mathcal{G}} \sum_{q \in \mathcal{N}(p)} w_{pq} V_{pq}(l_p, l_q)) \end{aligned} \tag{15}$$

where $\mathcal{E}$ is the set of edges connecting neighboring grid points and w_{pq} are the associated edge weights. V_p is the potential corresponding to the evaluation of the data term for grid point p and V_{pq} represents the pairwise potential corresponding to the cost of an edge.

Note that due to the equivalence of Gibbs Random Fields and Markov Random Fields[20,21] (MRFs), equation (15) represents the minimum of the posterior energy of the corresponding MRF.

Approximating the lowest potential, i.e. the global optimum, of such a MRF can be achieved with state-of-the-art graph-cut-based optimization algorithms such as α-expansion.[22] Our optimization is based on a recent graph-cut-based optimization technique[11,12] relying on duality theory of linear programming. Within this framework, a much wider class of MRFs can be handled than by α-expansion, while including α-expansion as a

special case. Furthermore, per-instance suboptimality bounds are provided. In practice, it turns out that these bounds are very tight,[12] the solution thus being very close to the global optimum of the MRF.

The optimization criterion being specified, we will now proceed to describe the algorithm, which embeds the minimization of equation (15) into a multiscale framework such that the motion is estimated in a coarse-to-fine manner. Image resolution, grid resolution as well as the displacement set capture range are successively refined: Different image resolution levels are obtained by computing a Gaussian pyramid on the input images. The different grid resolution levels are then defined by refining the initial grid point spacing according to the refinement of the image resolution in a higher pyramid level. To keep the optimization efficient, the set of displacements has to be small. Therefore, the search space during a single optimization cycle is restricted to displacements along the image axes. To ensure that the capture range of the search space is large enough for the dynamic range of all displacements to be estimated, the label set is successively refined in further optimization cycles. Note that due to this successive refinement, the resulting motion vectors are not restricted to lie on the image axes. Furthermore, within the MRF formulation of the registration problem we optimize the data terms grid point-wise. However, due to the support of cubic B-splines, the data terms of neighboring grid points cannot be computed independently of each other. Thus we approximate them by replacing the actual transformation τ by a simple shift such that for data term computation, the transformation is identical for all grid points.

4. EVALUATION

The evaluation of our approach relies on 3 time-lapse sequences, each one showing one cell. As a ground truth deformation field is not available, we chose the following twofold evaluation: The visual inspection of the estimated deformation field by an expert from cell biology combined with an evaluation of the evolution of the SSD.

In figure 4, one exemplary vector field estimate is illustrated superimposed to a 2D slice image that is cut out of the original 3D image. At the right hand part of the image one can easily see the postulated motion of the filaments from the cell periphery towards the interior. There is almost no motion at the left of the image because here the filaments are close to the nucleus. Considering the evaluation of the SSD, note that the images' bit-depth is 12 and that in all data sets, large parts do not contain structures of interest such that these parts cannot contribute to the improvement of the minimization criterion. Our evaluation shows the improvement of the mean SSD over the whole time series after registration, see RMSE in table 1. Additionally, we show how much the maximal squared difference has improved. To this end and in order to be robust against outliers, we compute the median over the 20 largest squared differences and show the mean over the whole time series in table 1.

Table 1. Evaluation of the RMSE and the median of the 20 largest squared differences before and after registration.

	Data set 1	Data set 2	Data set 3
RMSE before registration	191.3	3541.9	2499.8
RMSE after registration	142.3	2873.8	1957.7
Mean Median of max. diff. before registration	$13.29 \cdot 10^6$	$16.18 \cdot 10^6$	$13.01 \cdot 10^6$
Mean Median of max. diff. after registration	$11.05 \cdot 10^6$	$14.82 \cdot 10^6$	$11.18 \cdot 10^6$

5. CONCLUSIONS & FUTURE PROSPECTS

We have presented a novel approach for the three-dimensional motion analysis of keratin intermediate filaments which in principle can also be applied to other filamentous structures. The evaluation of the method has shown promising results that quantitatively support our hypothesis on keratin network dynamics. An important pre-processing step that has to be included in the future is Poisson denoising. Another future prospect is a physics based regularization functional. Furthermore, the FFD transformation model and the regularization we use for the smoothing of the deformation grid are not adapted to the handling of discontinuities at boundaries such

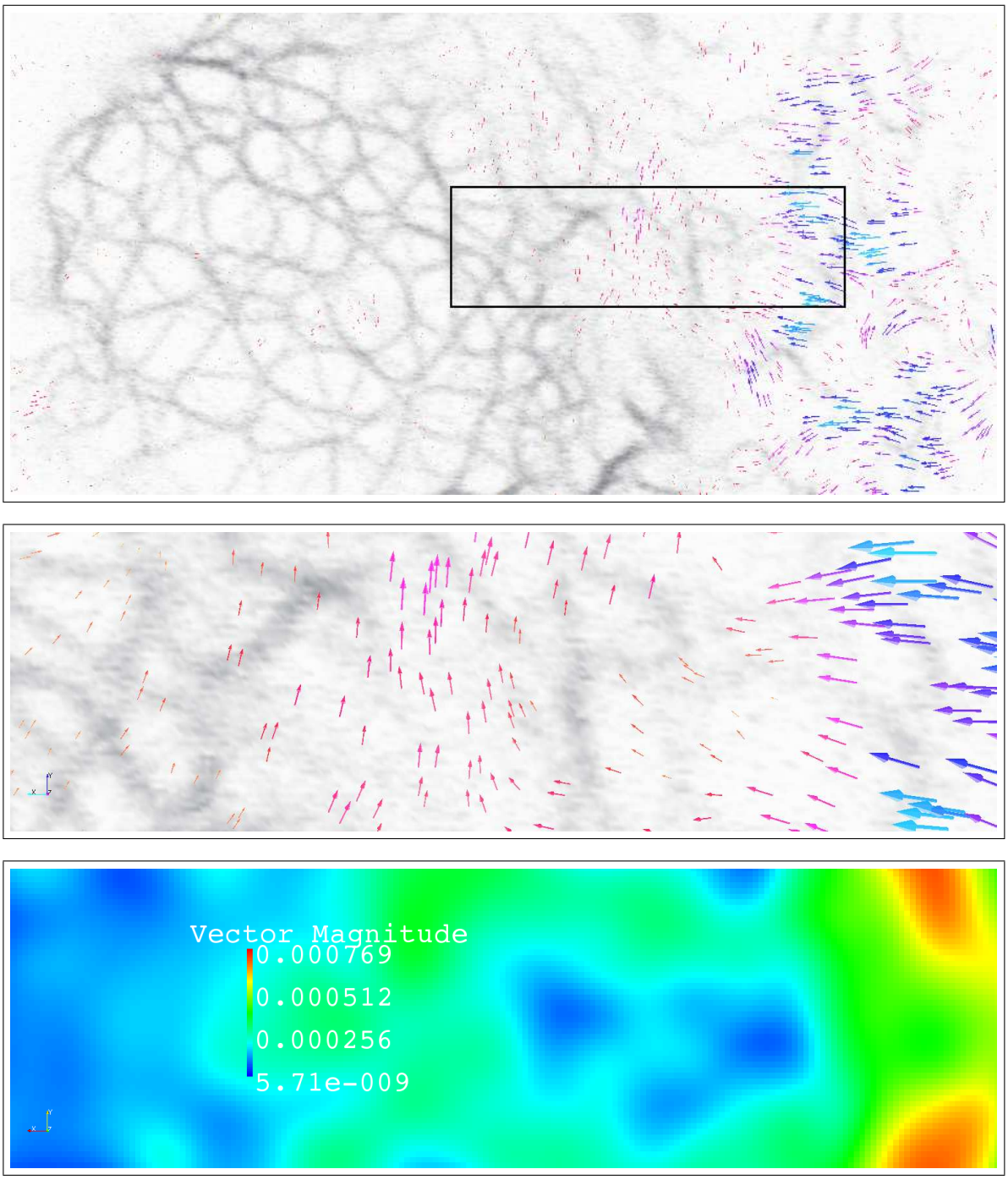

Figure 4. Cropped part of a 2D slice image of a cell. Top: Motion field estimate from t=9 min to t=10 min superimposed to original. For the sake of clarity, a threshold on the vector magnitude has been applied such that the motion field is only visualized for regions with significant motion. The box indicates the zoom area. Middle: Zoom of vector field superimposed to original. Bottom: Zoom of vector field magnitude in mm.

as the cell membrane and the nuclear membrane. Therefore, our goal is to combine the fluorescence data with phase contrast images that can simultaneuosly be acquired and indicate the location of object boundaries. Using this additional information, we can then include the handling of discontinuities in our model, leading to more precise results in the estimated vector fields.

ACKNOWLEDGMENTS

The work was supported by the German Research Council (LE 566/10, WI 731/6-1) and by the excellence initiative of the German federal and state governments.

REFERENCES

[1] Magin, T., Vijayaraj, P., and Leube, R., "Structural and regulatory functions of keratins.," *Exp Cell Res* **313(10)**, 2021–32 (2007).

[2] Windoffer, R., Woell, S., Strnad, P., and Leube, R. E., "Identification of novel principles of keratin filament network turnover in living cells.," *Mol Biol Cell* **15**, 2436–2448 (May 2004).

[3] Windoffer, R. and Leube, R. E., "De novo formation of cytokeratin filament networks originates from the cell cortex in a-431 cells.," *Cell Motil Cytoskeleton* **50**, 33–44 (Sep 2001).

[4] Klsch, A., Windoffer, R., and Leube, R. E., "Actin-dependent dynamics of keratin filament precursors.," *Cell Motil Cytoskeleton* **66**, 976–985 (Nov 2009).

[5] Danuser, G. and Waterman-Storer, C. M., "Quantitative fluorescent speckle microscopy of cytoskeleton dynamics.," *Annu Rev Biophys Biomol Struct* **35**, 361–387 (2006).

[6] Helmke, B. P., Thakker, D. B., Goldman, R. D., and Davies, P. F., "Spatiotemporal analysis of flow-induced intermediate filament displacement in living endothelial cells.," *Biophys J* **80**, 184–194 (Jan 2001).

[7] Raisch, F., Scharr, H., Kirchgener, N., Jaehne, B., Fink, R., and Uttenweiler, D., "Velocity and feature estimation of actin filaments using active contours in noisy fluorescence image sequences," in [*Visualization, Imaging, and Image Processing - 2002*], (2002).

[8] Glocker, B., Komodakis, N., Tziritas, G., Navab, N., and Paragios, N., "Dense image registration through MRFs and efficient linear programming," *Medical Image Analysis* **12**(6), 731–741 (2008).

[9] Glocker, B., Paragios, N., Komodakis, N., Tziritas, G., and Navab, N., "Optical flow estimation with uncertainties through dynamic mrfs," in [*Proc. IEEE Conference on Computer Vision and Pattern Recognition CVPR 2008*], 1–8 (2008).

[10] Rueckert, D., Sonoda, L. I., Hayes, C., Hill, D. L. G., Leach, M. O., and Hawkes, D. J., "Nonrigid registration using free-form deformations: application to breast MR images," *IEEE Transactions on Medical Imaging* **18**(8), 712–721 (1999).

[11] Komodakis, N., Tziritas, G., and Paragios, N., "Fast, approximately optimal solutions for single and dynamic MRFs," in [*Proc. IEEE Conference on Computer Vision and Pattern Recognition CVPR '07*], 1–8 (2007).

[12] Komodakis, N. and Tziritas, G., "Approximate labeling via graph cuts based on linear programming," *IEEE Transactions on Pattern Analysis and Machine Intelligence* **29**(8), 1436–1453 (2007).

[13] Pawley, J. B., ed., [*Handbook of Biological Confocal Microscopy*], Springer Verlag (2006).

[14] Windoffer, R. and Leube, R. E., "Imaging of keratin dynamics during the cell cycle and in response to phosphatase inhibition.," *Methods Cell Biol* **78**, 321–352 (2004).

[15] Dorn, J. F., Danuser, G., and Yang, G., "Computational processing and analysis of dynamic fluorescence image data.," *Methods Cell Biol* **85**, 497–538 (2008).

[16] Rohlfing, T., Maurer, C. R., J., Bluemke, D. A., and Jacobs, M. A., "Volume-preserving nonrigid registration of MR breast images using free-form deformation with an incompressibility constraint," *IEEE Transactions on Medical Imaging* **22**, 730–741 (June 2003).

[17] Bertero, M., Poggio, T. A., and Torre, V., "Ill-posed problems in early vision," *Proceedings of the IEEE* **76**, 869–889 (Aug. 1988).

[18] Terzopoulos, D., "Regularization of inverse visual problems involving discontinuities," *IEEE Transactions on Pattern Analysis and Machine Intelligence* , 413–424 (July 1986).

[19] Modersitzki, J., [*Numerical Methods for Image Registration*], Oxford University Press (2004).
[20] Li, S., [*Markov Random Field Modeling in Image Analysis*], Springer (2009).
[21] Geman, S. and Geman, D., "Stochastic relaxation, gibbs distributions, and the bayesian restoration of images," *IEEE Transactions on Pattern Analysis and Machine Intelligence* , 721–741 (Nov. 1984).
[22] Veksler, O., *Efficient Graph-Based Energy Minimization Methods In Computer Vision*, PhD thesis, Cornell University (1999).